AIP Journal of Applied Physics

Oxygen assisted interconnection of silver nanoparticles with femtosecond laser radiation

H. Huang, W. W. Duley, and Y. Zhou

Citation: Journal of Applied Physics **118**, 223101 (2015); doi: 10.1063/1.4937157
View online: http://dx.doi.org/10.1063/1.4937157
View Table of Contents: http://scitation.aip.org/content/aip/journal/jap/118/22?ver=pdfcov
Published by the AIP Publishing

Oxygen assisted interconnection of silver nanoparticles with femtosecond laser radiation

H. Huang,[1,2] W. W. Duley,[1,3] and Y. Zhou[1,2,a)]
[1]*Centre for Advanced Materials Joining, University of Waterloo, Waterloo, Ontario N2L 3G1, Canada*
[2]*Department of Mechanical and Mechatronics Engineering, University of Waterloo, Waterloo, Ontario N2L 3G1, Canada*
[3]*Department of Physics and Astronomy, University of Waterloo, Waterloo, Ontario N2L 3G1, Canada*

(Received 4 August 2015; accepted 22 November 2015; published online 8 December 2015)

Ablation of silver (Ag) nanoparticles in the direction of laser polarization is achieved by utilizing femtosecond laser irradiation in air at laser fluence ranging from ~2 mJ/cm^2 to ~14 mJ/cm^2. This directional ablation is attributed to localized surface plasmon induced localized electric field enhancement. Scanning electron microscopy observations of the irradiated particles in different gases and at different pressures indicate that the ablation is further enhanced by oxygen in the air. This may be due to the external heating via the reactions of its dissociation product, atomic oxygen, with the surface of Ag particles, while the ablated Ag is not oxidized. Further experimental observations show that the ablated material re-deposits near the irradiated particles and results in the extension of the particles in laser polarization direction, facilitating the interconnection of two well-separated nanoparticles. © *2015 AIP Publishing LLC*. [http://dx.doi.org/10.1063/1.4937157]

I. INTRODUCTION

Joining metallic nanomaterials into certain functional modules has attracted lots of attention, because this process can be used to precisely fabricate nanoelectronic and nanophotonic devices which have shown promising applications.[1–6] In the joining process, it is usually required to control the position of and limit the damage to the pre-joined nanomaterials. Joining nanomaterials via (bio)polymer molecules such as DNA can minimize the destruction of the nanomaterials and has shown some capacity of manipulating the pre-joined nanomaterials.[7,8] However, this joining process is complicated, and the relative low strength of the adhesive bonds between the polymer and the metallic nanomaterials weakens the stability of the final structures.

Joining by laser irradiation with laser pulse lengths exceeding one picosecond can produce robust metallic bonding between metallic nanomaterials but often faces the challenge of minimizing damage to the pre-joined nanomaterials.[9–14] Recently, a new femtosecond (fs) laser nanojoining technique has shown promise in solving this issue, because of its small thermal damage to irradiated nanomaterials.[15,16] It has been reported that, with fs laser radiation in vacuum (10^{-6} Torr), two adjacent Ag nanoparticles (NPs), separated by ~30 nm, could be interconnected through the re-deposition of locally ablated material, while the geometries of the interconnected particles remained almost intact.[16] The required small separation distance and the need for high vacuum are two potential limitations in this technique in industrial applications.[16]

One possible solution is to employ a reactive gas to assist the joining process. The role of this gas is to improve the absorption of laser energy[17] or to enhance heat generation through chemical reaction with the pre-joined materials,[18] which then accelerates the re-deposition process due to the increased amount of locally ablated material. In this work, we have studied the influence of gases (specifically O_2) on the morphology of fs laser irradiated Ag NPs on a Si wafer and have investigated their overall contribution to the interconnection of these particles. We have identified the role played by localized surface plasmon (LSP) induced electric field enhancement in hotspots in the interconnection process.

II. EXPERIMENTAL AND SIMULATION

Ag NPs were deposited on a Si wafer (as received, MRS material) by fs laser ablation of an Ag target at a fluence approximately 1.4 J/cm^2, as reported previously.[16] The particles lie with their flat surface in contact with the Si substrate, which is similar to an elliptic cylinder with an axis ratio of 1.08 ± 0.06 (based on 200 measurements) and a height to diameter ratio of 2.8 ± 0.6 (based on 45 AFM measurements). The size distribution of these particles is in the range between 50 and 600 nm (Fig. 1). In the following data, particles with sizes <50 nm are not counted because it is difficult to distinguish the change in morphology of these particles before and after fs laser radiation. The laser with 800 nm wavelength, 35 fs pulse duration, and 1 kHz repetition rate is manufactured by Coherent Inc. The laser operates in the TEM_{00} with $M^2 < 1.3$ and a beam diameter of 6 mm. This effectively covers the entire irradiated Si wafer.

After deposition, the particles on the Si surface were then irradiated using the same fs laser at fluences between 2 and 14 mJ/cm^2 for different times. Different gases (air, nitrogen (N_2), and O_2) and pressures (760, 10^{-2}, 1, and 10^{-4} Torr) were used to identify the influence of the gases on the morphology of fs laser irradiated particles. The morphology of the irradiated Ag NPs was analyzed by scanning electron microscope (SEM, LEO 1550), and the cross-section of the interconnected particles was studied by transmission electron microscope (TEM, JEOL-2010F) which is equipped with

a)Electronic mail: nzhou@uwaterloo.ca

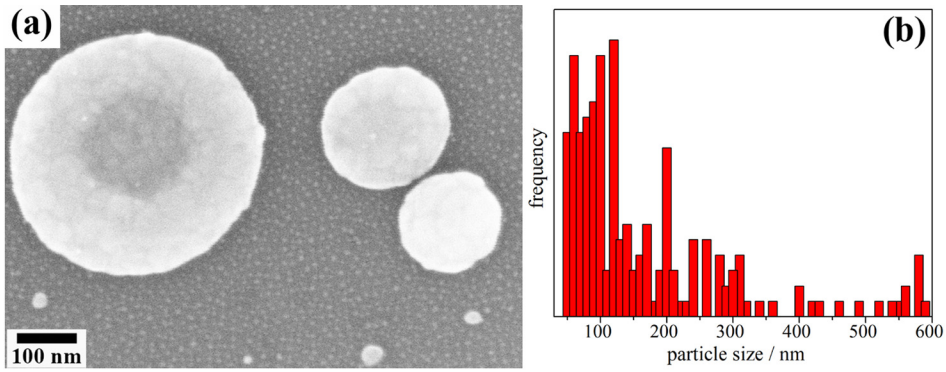

FIG. 1. SEM morphology (a) and size distribution (b) of deposited Ag particles.

energy dispersive X-ray spectrometer (EDS, Oxford). Commercial FDTD software (Lumerical Solutions) was used to identify the electric field enhancement in the Ag particles irradiated at 800 nm.

III. RESULTS AND DISCUSSIONS

To study the feasibility of obtaining high integrity interconnection of Ag NPs at atmospheric pressure rather than in high vacuum (10^{-6} Torr),[16] Ag NPs were irradiated with fs laser pulses at pressures ranging from 1.3×10^{-4} Torr to 760 Torr. SEM images of the morphology of irradiated particles show that, at pressures of 1.3×10^{-4} and 1.7×10^{-2} Torr (Figs. 2(a) and 2(b)), Ag NPs were ablated in the two pole areas which were parallel to the direction of the laser polarization. The size distribution of these ablated particles was centered between 60 and 150 nm (Fig. 2(c)). This can be attributed to hotspot-enhanced localized ablation in the pole areas due to the excitation of LSPs.[19] The ablated material then re-deposited nearby forming "tabs," and resulting in the extension of the particle in the direction of the laser polarization. The *L*/*D* ratio compares the length of the "tab" *L* (indicated by the red dashed line in the figure) to the particle diameter *D*. This ratio is used to characterize the ablation

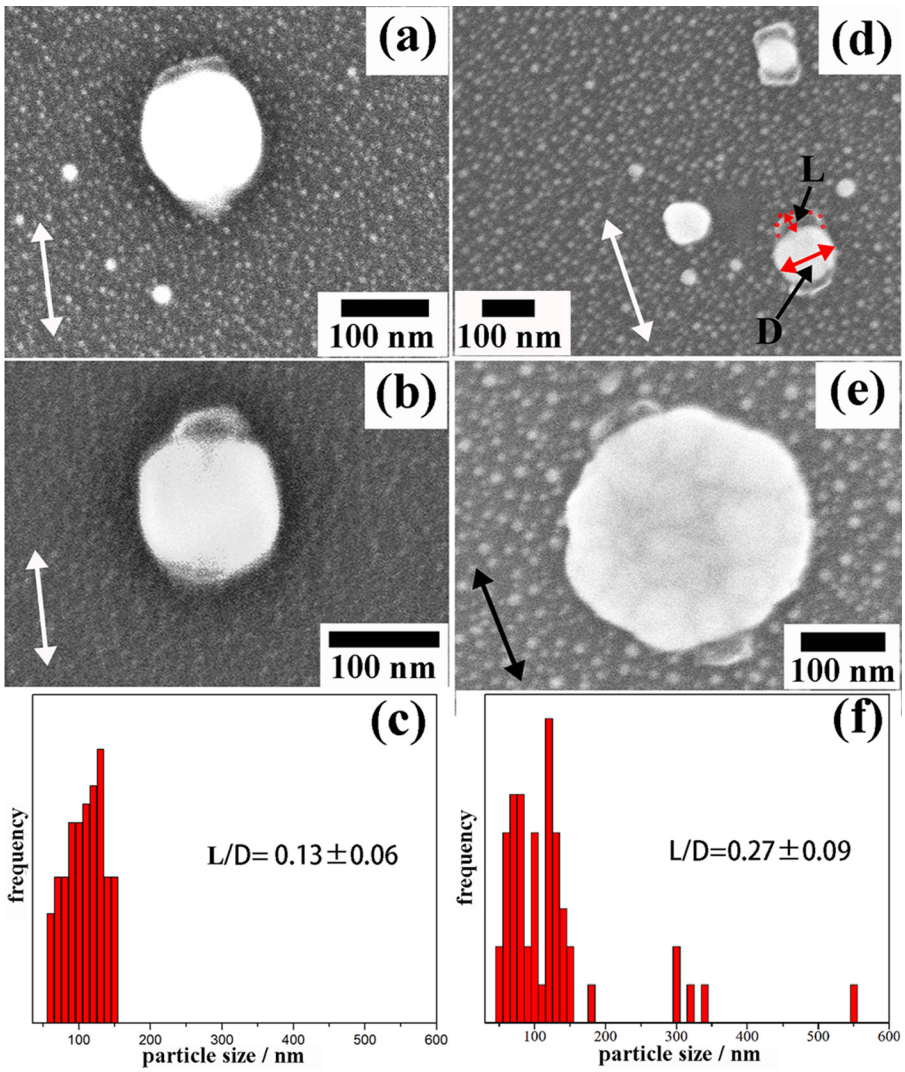

FIG. 2. SEM morphology and size distribution of the particles ablated by fs laser irradiation at fluence 7.2 mJ/cm^2 for 10 s at different pressures. (a) 1.3×10^{-4} Torr, (b) 1.7×10^{-2} Torr, (c) size distribution of the particles irradiated at 1.7×10^{-2} Torr, (d) and (e) 760 Torr, and (f) size distribution of the particles irradiated at 760 Torr. The double-end arrows show the direction of laser polarization.

behavior of irradiated NPs at different atmospheric pressures and minimizes the effect of particle size. This ratio is 0.13 ± 0.06 based on measurements for 50 particles as shown in Fig. 2(c), at a pressure 1.7×10^{-2} Torr. This directional extension of Ag NPs shows the potential for interconnecting well-separated particles. When the particles were irradiated at 760 Torr, similar "tab" structures were obtained (Figs. 2(d) and 2(e)), and the *L*/*D* ratio increased to 0.27 ± 0.09 (based on 50 particles, the size distribution of these particles is shown in Fig. 1(f)). This suggests that an increase in air pressure enhanced the ablation of the particles in the direction of the laser polarization.

It should be noted that selective ablation was also observed in particles with sizes exceeding 300 nm (Figs. 2(e) and 2(f)). As it can be shown that the enhancement factor in LSP-induced hotspots, which contribute to the ablation of irradiated particles, is much reduced in large particles (>300 nm) compared to that in particles with sizes between 50 and 150 nm; ablation in larger particles is probably due to an LSP-triggered reaction. Since air consists of 21% oxygen (O_2) and 78% nitrogen (N_2), by volume, we have investigated the contribution of each of these gases by irradiating Ag particles at atmospheric pressure in pure N_2 and O_2. SEM images of the morphology of Ag particles irradiated in N_2 (Fig. 3(a)) and O_2 (Fig. 3(b)) indicate that ablation is enhanced in O_2 compared to N_2. The *L*/*D* ratio in N_2, 0.12 ± 0.03, was close to that in vacuum, while the ratio in O_2 (0.21 ± 0.04) was much larger than that in N_2 and close to that in air. These results imply that O_2 plays a dominant role in enhancing the ablation of Ag nanoparticles under fs laser irradiation.

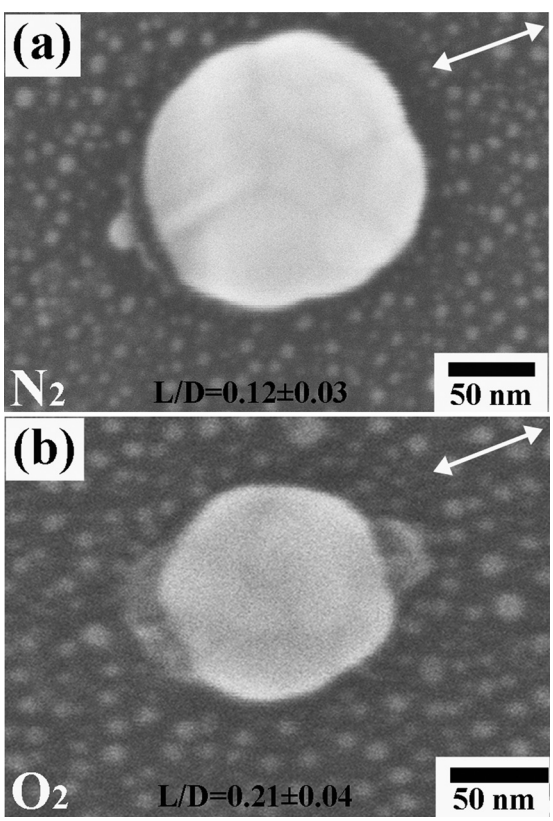

FIG. 3. Images of the morphology for Ag NPs after irradiation by fs laser pulses for 10 s in N_2 (a) and O_2 (b). The double-end arrows show the direction of laser polarization.

The reaction between O_2 and Ag is negligible at room temperature,[20] suggesting that laser radiation initiates the reaction of O_2 with Ag. Three intensity dependent interaction regimes, corresponding to multi-photon dissociation (total energy <5.2 eV) or ionization (total energy <12.1 eV) of O_2, have been reported.[21,22] These are

$$O_2 + n\,h\nu \rightarrow O + O, \tag{1}$$

$$O_2 + m\,h\nu \rightarrow O_2^+ + e^-, \tag{2}$$

$$O + l\,\mathrm{hv} \rightarrow O^+ + e^-, \tag{3}$$

where *n*, *m*, and *l* are the numbers of the laser photons absorbed by O_2 molecules in the dissociation (Equation (1)) and ionization (Equations (2) and (3)) processes. The threshold energy for the dissociation of O_2 (Equation (1)) is 5.2 eV,[23] while those for ionization of O_2 (Equation (2)) and O (Equation (3)) are 12.1 eV and 13.6 eV,[24,25] respectively. This indicates that the dissociation of O_2 dominates the interaction relative to ionization of O_2 and O in the laser–O_2 interaction. Here, the photon energy is 1.55 eV, and absorption of five photons is needed to dissociate O_2.[21] After the dissociation of O_2, energetic O atoms will possess a kinetic energy of 1.28 eV which is half the energy remaining following the absorption of five laser photons and dissociation of the molecule. These energetic atoms impact and react to form an oxide at the surface of the Ag particle. Assuming that all the kinetic energy of the O atom is released in its reaction with the surface of Ag particle, possible reactions between O and Ag are[26,27]

$$O + 2Ag \rightarrow Ag_2O + 154.6\,\mathrm{kJ/mol}, \tag{4}$$

$$O + Ag_2O \rightarrow (AgO)_2 + 116.7\,\mathrm{kJ/mol}, \tag{5}$$

$$O + (AgO)_2 \rightarrow Ag_2O + O_2 + 130.3\,\mathrm{kJ/mol}. \tag{6}$$

Equations (4)–(6) clearly show that these reactions are highly exothermic so it can be expected that some of this energy will result in localized heating in the Ag particle. Due to its low decomposition temperature (~190 °C), Ag_2O will decompose if the temperature increase in reaction (4) exceeds 190 °C. Since reactions (5) and (6) occur only after the formation of Ag_2O these may not take place in the fs laser radiation process. The decomposition of Ag_2O can be written as

$$Ag_2O \rightarrow 2Ag + \frac{1}{2}O_2 - 31.1\,\mathrm{kJ/mol}, \tag{7}$$

which is endothermic by ~31 kJ/mol. The reverse reaction (7) then becomes dominant as the temperature of the Ag particle increases. As we find that no Ag oxides are detected on the particles after irradiation, the reverse reaction must occur at a sufficient rate to preclude the accumulation of oxide. The overall reaction is then

$$2O \xrightarrow{Ag} O_2 + 247\,\mathrm{kJ/mol}. \tag{8}$$

This suggests that the enhancement in local heating in fs laser irradiated Ag particles arises from the surface recombination of O atoms to form O_2. It also implies that the degree of local heating enhancement will then depend on the density of O atoms at the surface of the Ag particle and will be a function of gas pressure and laser fluence.

As shown in Fig. 4(a), with the increase of N_2 pressure from 10^{-2} Torr to 760 Torr, the *L*/*D* ratio of Ag particles which were irradiated by fs laser at a fluence approximately 10 mJ/cm^2 for 10 s was ~0.16–0.2. The absence of a strong effect of pressure on *L*/*D* ratio arises because N_2 does not react with Ag particles. A significant variation of the *L*/*D* ratio was observed when the Ag particles were irradiated by fs laser at different air pressures (corresponding to different O_2 density). To quantify these effects, Fig. 4(b) shows the change in the *L*/*D* ratio with O_2 density at a constant laser fluence of 7.2 mJ/cm^2 and irradiation time of 10 s. It is apparent that increasing the O_2 density from 6×10^{11}/cm^3 (1×10^{-4} Torr) to 6×10^{15}/cm^3 (1 Torr) results in an increase in the average *L*/*D* ratio from 0.1 to 0.25. A further increase in density to 5×10^{17}/cm^3 (760 Torr) produces only a slight rise in the average *L*/*D* ratio to 0.27. This implies that, at a given fs laser fluence, the number density of O atoms generated from the dissociation of O_2 saturates above a critical O_2 density. In this regime, the number density of O atoms will increase with laser fluence.[16]

Fig. 4(c) shows the measured *L*/*D* as a function of laser fluence at constant O_2 densities of 5×10^{17}/cm^3 (760 Torr) and 6×10^{11}/cm^3 (1×10^{-4} Torr). It can be seen that the *L*/*D* ratio increases along with laser fluence at both O_2 densities. The rate of increase of the *L*/*D* ratio at a density of 5×10^{17}/cm^3 is much faster than that at 6×10^{11}/cm^3 for fluences exceeding 7.2 mJ/cm^2. At a density of 6×10^{11}/cm^3, the *L*/*D* ratio approaches ~0.2 as the laser fluence is varied from ~4 mJ/cm^2 to ~14 mJ/cm^2 because the O_2 density is much lower than the critical concentration, and the *L*/*D* ratio is therefore density limited.

To better understand the evolution of Ag NPs under fs laser radiation in air, changes in particle morphology as a function of irradiation time are shown in Fig. 5. Relatively high fluence (~14 mJ/cm^2) was used in order to obtain noticeable changes in morphology in the irradiated paticles in short irradiation time. Fig. 5(a) shows that after 1 s, a "tab" structure develops on the irradiated particle without any apparent damage. This is similar to the structures shown in Figs. 2–3. With an increase in irradiation time to 4 s (Fig. 5(b)), particles are partially ablated, and some particles are ejected following laser irradiation leaving holes in the Si wafer, as shown in the inset in Fig. 5(b). Because the laser fluence was much lower than the damage threshold fluence of the Si wafer,[28] the holes in the Si wafer were caused by enhanced ablation in LSP-induced hotspots as reported previously.[13] This implies that particle ablation starts from the bottom edge on the surface where the electric field enhancement is highest. Further increases in irradiation time to 7 s (Fig. 5(c)) and 10 s (Fig. 5(d)) produce more extensive ablation, and the particles are seen to extend in the direction of laser polarization direction due to the re-deposition of ablated material. This effect enables the joining of separated Ag NPs.

Since NPs are found to extend in the direction of laser polarization due to the accumulation of ablated material, this suggests that this effect has the potential for interconnecting separated particles in the assembly of nanodevices. Fig. 6(a) shows that the separation distance between two Ag particles was reduced due to the accumulation of re-deposited material in the laser polarization direction after fs laser radiation for 10 s at a fluence of ~7.2 mJ/cm^2. Some Ag particles are found to be connected in this way even when the separation distance was ill-defined as shown in Fig. 6(b). Ag particles

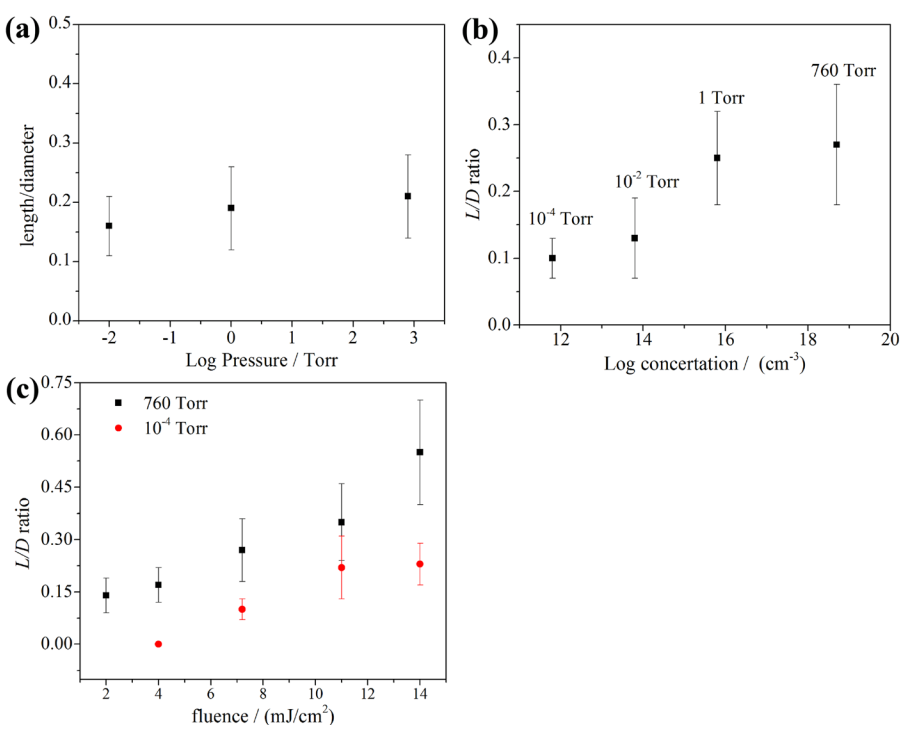

FIG. 4. Effects of gas source and gas density (or pressure) on *L*/*D* ratio. (a) Correlation between *L*/*D* ratio and N_2 pressure, the laser fluence is constant at 10 mJ/cm^2, and the irradiation time is 10 s. (b) Correlation between *L*/*D* ratio and O_2 density. The laser fluence is constant at 7.2 mJ/cm^2, and the irradiation time is 10 s; (c) correlation between *L*/*D* ratio and laser fluence at two O_2 densities (correspond to air pressures 10^{-4} Torr and 760 Torr).

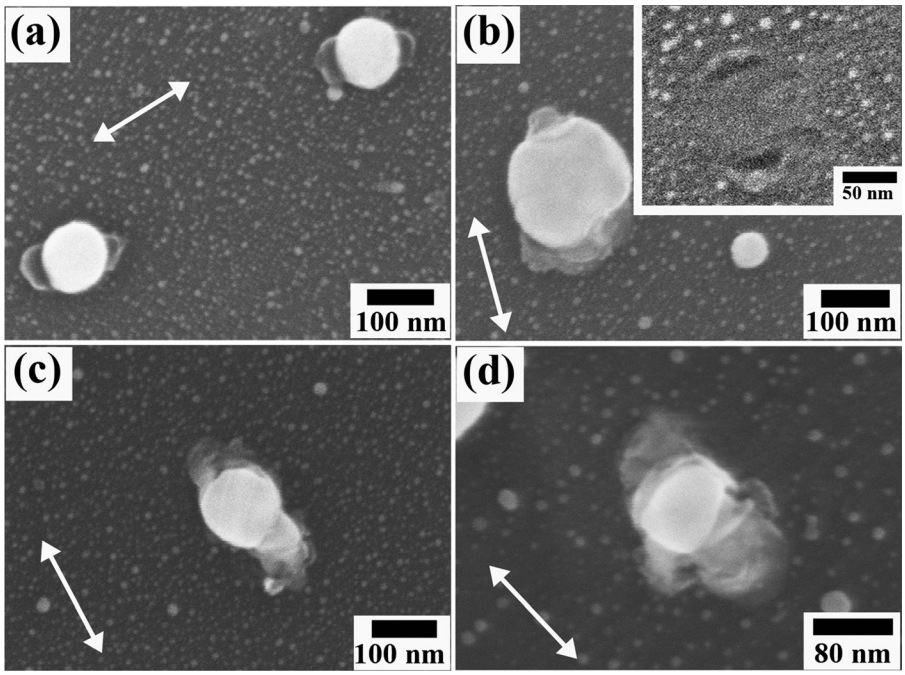

FIG. 5. SEM images of the morphology for the Ag NPs which were irradiated by fs laser at fluence 14 mJ/cm^2 for different times. (a) 1 s; (b) 4 s, the inset image shows the holes in the Si wafer; (c) 7 s; (d) 10 s. The double-end arrows show the direction of laser polarization.

with a large separation distance (~180 nm) could also be connected after increasing the irradiation time to 50 s (Figs. 6(c) and 6(d)). The interconnecting bridge is formed via the accumulation and sintering of ablated material between the initial particles. An increase in irradiation time results in the further accumulation of re-deposited material between the separated particles, facilitating the interconnection of particles with large separation distance. This is reflected in an increase in the ratio of the total length L_1 of the irradiated particle and its diameter D with irradiation time. The measurement of L_1 and D is shown in Fig. 6(e). Fig. 6(f) shows that, at fs laser fluence ~7.2 mJ/cm^2, the L_1/D ratio changed from 1.1 to a constant value of ~1.54 when the irradiation time was increased from 0 to 70 s.

At higher fluence, the sintering of the re-deposited material in the interconnection area became more pronounced due to high energy input, and a more compact joint structure was obtained. This dense structure can be seen in Fig. 7(a), in the interconnection between two Ag particles with diameters of 430 nm and 500 nm separated by 110 nm. The high fluence did not cause serious destruction of the particles except in the pole areas parallel to the laser polarization direction. Figs. 7(b) and 7(c) show TEM images of the cross-sectional morphology in the interconnected area. It can be seen that the two Ag particles are connected via an accumulation of re-deposited material. This is reflected in the appearance of a noticeable bonding interface between the Ag particle and the re-deposited material (Fig. 7(d)). The presence of re-deposited material in the Si wafer suggests that the ablated material came from the ablation of both the Ag particles and the wafer as the result of localized heating. EDS analyses in the interconnected area show that Si and O are present close to the Ag particle. The ratio between Si and O atoms was ~1 (EDS spots A, B, C in Fig. 7(c)). This ratio is close to that in the SiO_x ($x < 2$) layer on the surface of the Si wafer,[29] suggesting that this material came from the ablation of Si. In the center of the interconnection, the material consists mainly of Ag with a small amount of Si together with a small amount of O (EDS spots D in Fig. 7(c)). This indicates that there was little retention of oxide resulting from the Ag/O reaction. This is consistent with the above analysis and reveals that no Ag_2O is present in the ablated material. Based on this result, we conclude that O_2 assisted fs laser processing can be used to join well-separated Ag particles without causing oxidation. This method then has potential for applications in the fabrication of nanoscale electronic devices. As noted, Si in the re-deposited material comes from ablation of the Si wafer. The presence of Si in the interconnection will influence the strength and electrical conductivity of the joint. Figs. 7(d) and 7(e) show HRTEM images of the morphology in the interconnection at positions A and D, respectively. A clear bonding interface between the particle and the re-deposited material was observed in the area close to the particle (Fig. 7(d)), while pure Ag-Ag metallic bonding could also be obtained in the center of the interconnection, suggesting that complete metallic bonding between the irradiated Ag NPs could be obtained if Si contamination can be eliminated.

To reduce the influence of Si on the joint strength and electric conductivity, the ablation of the Si wafer can be minimized by adjusting the location of LSP-induced hotspots within the irradiated Ag particles. Fig. 8(a) shows a simulation of the distribution of hotspots in two irradiated Ag particles similar to those appearing in Fig. 7(a). For simplification, these particles are taken to be elliptic cylinders with heights of 121 nm and 130 nm, respectively. This simulation reveals the presence of hotspots in each particle near the surface of the Si wafer and is consistent with the experimental observation of ablation in the Si wafer (Fig. 7). Changing the height of each cylinder to 180 nm yields the field distribution shown in Fig. 8(b) and eliminates the hotspots at the surface of the Si wafer.

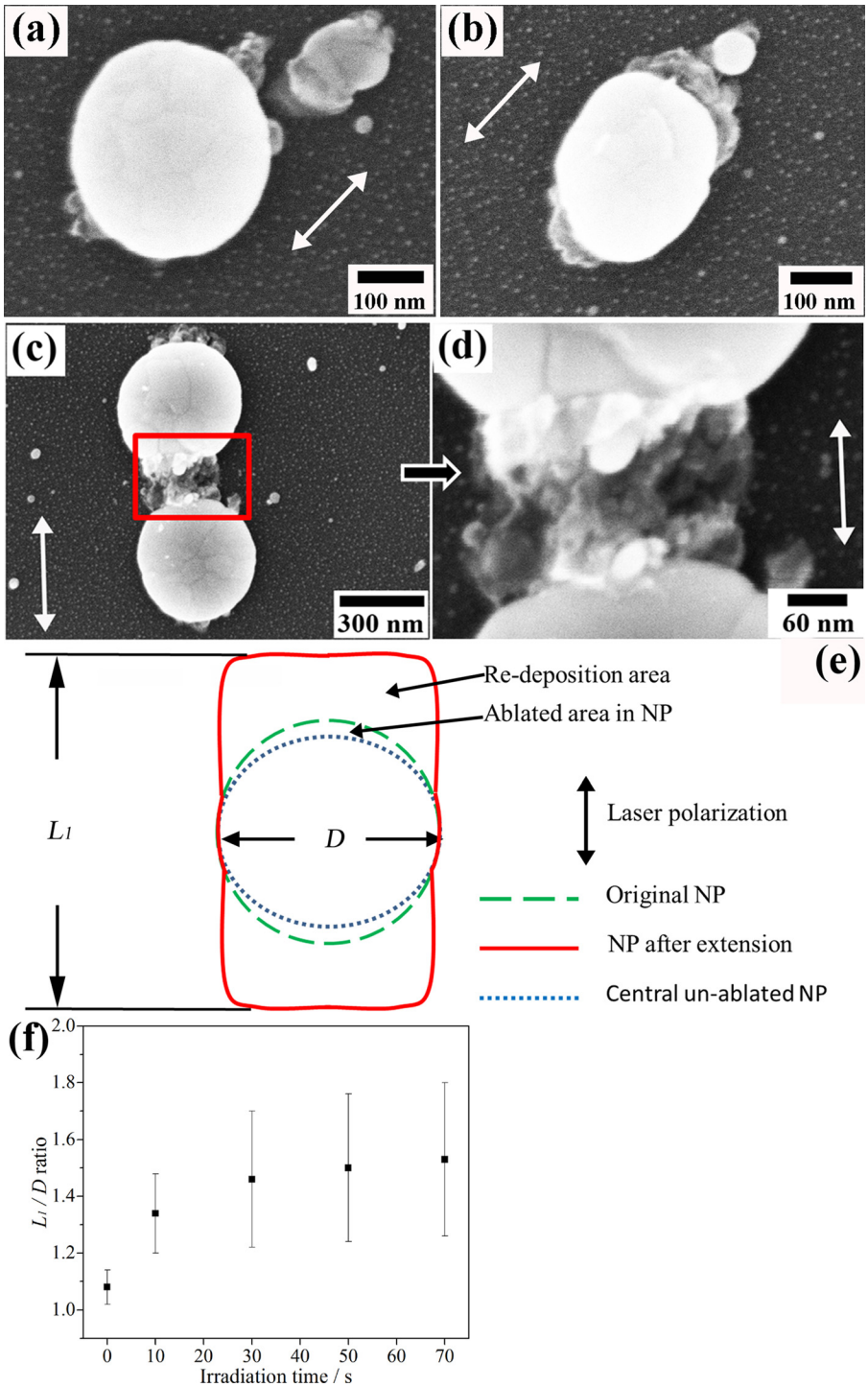

FIG. 6. SEM images showing the morphology of Ag NPs which were irradiated by fs laser pulses at a fluence 7.2 mJ/cm^2 for different times. (a) Closely spaced particles after 10 s radiation, (b) interconnected particles after 10 s irradiation, (c) interconnected particles after 50 s irradiation, (d) magnified view of the square area in (c). The double ended arrows show the direction of laser polarization. (e) Definition of the measurement of length of irradiated particles in the laser polarization direction and the original diameter. (f) Correlation of L_1/D ratio with irradiation time.

This simple modification will inhibit the ablation of Si and prevent Si from being incorporated in the interconnecting material, leading to an improvement in the strength and electrical conductivity of the connecting bridge. Other methods, such as changing the incident laser wavelength and the separation distance between two particles, may also be used to tailor the location of hotspots. Experimental work in this area is on-going, and will be reported later.

IV. CONCLUSION

In this work, it is demonstrated that Ag NPs can be selectively ablated in the direction of the laser polarization by fs laser irradiation in air. This effect arises from the excitation of LSP-induced hotspots. It is believed that dissociation of gas phase O_2 is facilitated in the vicinity of the hotspots producing O atoms that react with Ag particles. The exothermicity of this reaction heats the Ag surface and enhances ablation in the region of the hotspots. Ablated material re-deposits near the irradiated particles and results in their spatial extension along the direction of the laser polarization. This process can be used to facilitate the interconnection of adjacent Ag NPs. TEM analysis of the cross-sectional morphology for interconnected Ag particles indicates that Ag oxides are not present in the bridge between the two particles. The presence of SiO_x and Si in

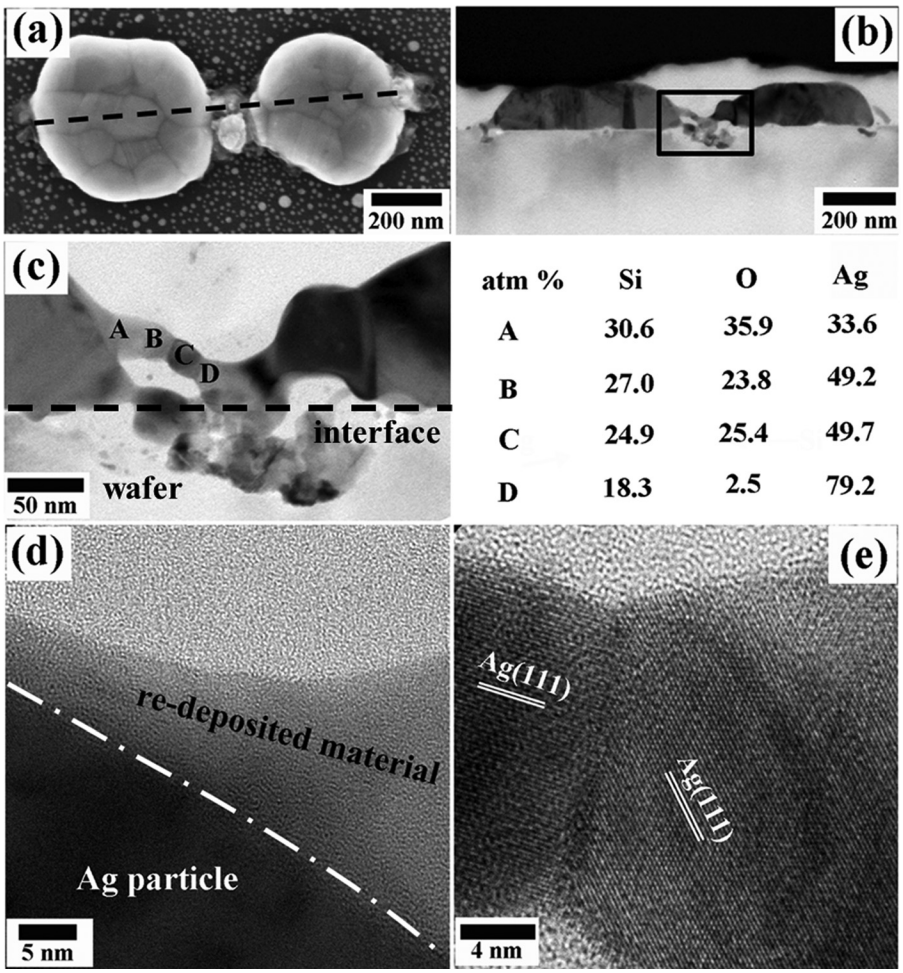

FIG. 7. SEM and TEM analyses of Ag NPs after irradiation by fs laser pulses at a fluence of 11 mJ/cm^2 for 10 s. (a) SEM image of the morphology of Ag particles, the double-ended arrow shows the direction of laser polarization; (b) TEM image of the cross-section of the particles along the dashed line; (c) enlargement of the area 1 in (b) and corresponding EDS analyses at locations A, B, C, D; (d) HRTEM image at location A in (c); (e) HRTEM image at location D in (c).

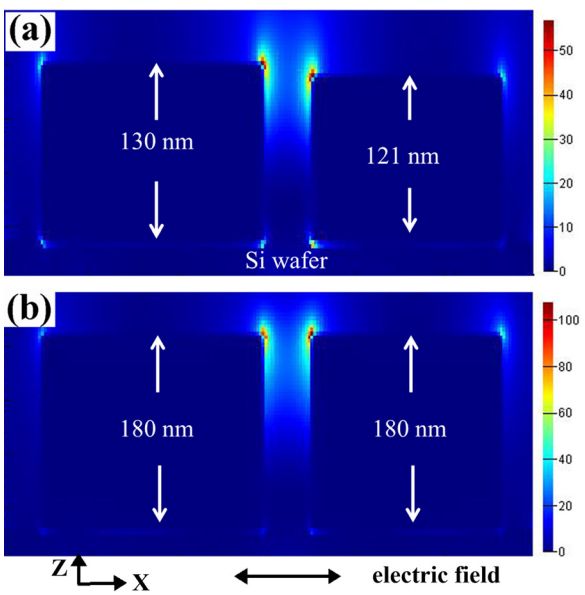

FIG. 8. Electric field distribution showing LSP-induced hotspots in two different structures. (a) Simulation of field in the vicinity of two adjacent Ag elliptic cylinders. The left elliptic cylinder has D1 = 500 nm, D2 = 470 nm and H = 130 nm, while the right cylinder has D = 430 nm and H = 121 nm; (b) as in (a), but with H = 180 nm. The laser beam is incident in the Z-direction, and the double-ended arrow shows the direction of the optical electric field.

this bridging material is due to ablation of the underlying Si wafer and can be minimized by tailoring the size and shape of adjacent particles as well as by adjustments in irradiation conditions.

ACKNOWLEDGMENTS

The work is financially supported from the National Sciences and Engineering Research Council of Canada (NSERC) and the State Scholarship Fund of China (No. 2011640021). The authors would like to thanks Dr. Mugunthan Sivayoganathan at Centre for Advanced Materials Joining, University of Waterloo, for helpful discussions.

[1]J. Lee, P. Lee, H. B. Lee, S. Hong, I. Lee, J. Yeo, S. S. Lee, T. Kim, D. Lee, and S. H. Ko, Adv. Funct. Mater. **23**, 4171 (2013).
[2]W. Lu and C. M. Lieber, Nat. Mater. **6**, 841 (2007).
[3]F. N. Xia, L. Sekaric, and Y. Vlasov, Nat. Photonics **1**, 65 (2007).
[4]J. Lee, P. Lee, H. Lee, D. Lee, S. S. Lee, and S. H. Ko, Nanoscale **4**, 6408 (2012).
[5]S. Hong, J. Yeo, G. Kim, D. Kim, H. Lee, J. Kwon, H. Lee, P. Lee, and S. H. Ko, ACS Nano **7**, 5024 (2013).
[6]J. Yeo, S. Hong, D. Lee, N. Hotz, M. Lee, C. P. Grigoropoulos, and S. H. Ko, PLoS One **7**, e42315 (2012).
[7]H. Yao, C. Q. Yi, C. H. Tzang, J. J. Zhu, and M. S. Yang, Nanotechnology **18**, 015102 (2007).
[8]M. Grzelczak, J. Vermant, E. M. Furst, and L. M. Liz-Marzan, ACS Nano **4**, 3591 (2010).
[9]S. Xu, M. Tian, J. Wang, J. Xu, J. M. Redwing, and M. H. Chan, Small **1**, 1221 (2005).

[10]A. Hu, J. Y. Guo, H. Alarifi, G. Patane, Y. Zhou, G. Compagnini, and C. X. Xu, Appl. Phys. Lett. **97**, 153117 (2010).
[11]H. Tohmyoh, T. Imaizumi, H. Hayashi, and M. Saka, Scr. Mater. **57**, 953 (2007).
[12]S. H. Ko, H. Pan, D. J. Hwang, J. Chung, S. Ryu, C. P. Grigoropoulos, and D. Poulikakos, J. Appl. Phys. **102**, 093102 (2007).
[13]H. Pan, D. J. Hwang, S. H. Ko, T. A. Clem, J. M. J. Frechet, D. Bauerle, and C. P. Grigoropoulos, Small **6**, 1812 (2010).
[14]J. Chung, S. Han, D. Lee, S. Ahn, C. P. Grigoropoulos, J. Moon, and S. H. Ko, Opt. Eng. **52**, 024302 (2013).
[15]H. Huang, L. Liu, P. Peng, A. Hu, W. W. Duley, and Y. Zhou, J. Appl. Phys. **112**, 123519 (2012).
[16]H. Huang, M. Sivayoganathan, W. W. Duley, and Y. Zhou, Nanotechnology **2**, 025303 (2014).
[17]T. Ditmire, R. A. Smith, J. W. G. Tisch, and M. H. R. Hutchinson, Phys. Rev. Lett. **78**, 3121 (1997).
[18]M. Sobih, P. L. Crouse, and L. Li, J. Phys. D: Appl. Phys. **40**, 6908–6916 (2007).
[19]A. Plech, V. Kotaidis, M. Lorenc, and J. Boneberg, Nat. Phys. **2**, 44 (2006).
[20]W. A. Czanderna, J. Phys. Chem. **68**, 2765 (1964).
[21]S. Yang, W. T. Hill III, and S. N. J. Dixit, Chem. Phys. **100**, 6434 (1994).
[22]A. L'Huillier, G. Mainfray, and P. M. Johnson, J. Chem. Phys. Lett. **103**, 447 (1984).
[23]Y. R. Luo, *Comprehensive Handbook of Chemical Bond Energies* (CRC Press, 2007).
[24]R. J. Dewhurst, J. Phys. D: Appl. Phys. **11**, L191 (1978).
[25]D. R. Lide, *CRC Handbook of Chemistry and Physics* (CRC Press, 1992), p. 10–211.
[26]A. L. Myerson, J. Chem. Phys. **38**, 2043 (1963).
[27]A. L. Myerson, J. Chem. Phys. **42**, 3270 (1965).
[28]H. O. Jeschke, M. E. Garcia, M. Lenzner, J. Bonse, J. Kruger, and W. Kautek, Appl. Surf. Sci. **197–198**, 839 (2002).
[29]A. H. Al-Bayati, K. G. Orrman-Rossiter, J. A. van den Berg, and D. G. Armour, Surf. Sci. **241**, 91 (1991).